Clim Dyn (2014) 43:2985–2997
DOI 10.1007/s00382-014-2061-4

The Equatorial Undercurrent in the central Atlantic and its relation to tropical Atlantic variability

Peter Brandt · Andreas Funk · Alexis Tantet · William E. Johns · Jürgen Fischer

Received: 2 May 2013 / Accepted: 21 January 2014 / Published online: 1 February 2014

Abstract Seasonal to interannual variations of the Equatorial Undercurrent (EUC) in the central Atlantic at 23°W are studied using shipboard observation taken during the period 1999–2011 as well as moored velocity time series covering the period May 2005–June 2011. The seasonal variations are dominated by an annual harmonic of the EUC transport and the EUC core depth (both at maximum during September), and a semiannual harmonic of the EUC core velocity (maximum during April and September). Substantial interannual variability during the period of moored observation included anomalous cold/warm equatorial Atlantic cold tongue events during 2005/2008. The easterly winds in the western equatorial Atlantic during boreal spring that represent the preconditioning of cold/warm events were strong/weak during 2005/2008 and associated with strong/weak boreal summer EUC transport. The anomalous year 2009 was instead associated with weak preconditioning and smallest EUC transport on record from January to July, but during August coldest SST anomalies in the eastern equatorial Atlantic were observed. The interannual variations of the EUC are discussed with respect to recently described variability of the tropical Atlantic Ocean.

Keywords Equatorial Atlantic circulation · Moored and shipboard observations · Cold tongue · Seasonal cycle · Interannual variability · African monsoon

This paper is a contribution to the special issue on tropical Atlantic variability and coupled model climate biases that have been the focus of the recently completed Tropical Atlantic Climate Experiment (TACE), an international CLIVAR program (http://www.clivar.org/organization/atlantic/tace). This special issue is coordinated by William Johns, Peter Brandt, and Ping Chang, representatives of the TACE Observations and TACE Modeling and Synthesis working groups.

P. Brandt (✉) · A. Tantet · J. Fischer
GEOMAR Helmholtz-Zentrum für Ozeanforschung Kiel, Kiel, Germany
e-mail: pbrandt@geomar.de

A. Funk
WTD 71/FWG, Forschungsbereich für Wasserschall und Geophysik, Kiel, Germany

Present Address:
A. Tantet
Institute for Marine and Atmospheric Research, Utrecht University, Utrecht, The Netherlands

W. E. Johns
RSMAS/MPO, University of Miami, Miami, FL, USA

1 Introduction

The Equatorial Undercurrent (EUC) is among the strongest currents of the tropical ocean (Cromwell et al. 1954; Metcalf et al. 1962). It is generated at the subsurface under predominantly Easterlies in the equatorial Pacific and Atlantic Oceans and flows opposite to the wind following the depth-dependent eastward pressure gradient. The full three-dimensional structure of the EUC, which can only be explained by including viscous and inertial effects, is associated with strong horizontal flow divergences that are particularly responsible for the supply of the eastern equatorial upwelling (Qiao and Weisberg 1997; Schott et al. 1998). In the Atlantic, the EUC is supplied almost exclusively from the southern hemisphere. It transports oxygen-rich and high-saline water masses from the western boundary eastward (Metcalf et al. 1962; Schott et al. 1998; Kolodziejczyk et al. 2009; Brandt et al. 2011a). The transport of the Atlantic EUC contributes to both the

equator-crossing warm water pathway of the meridional overturning circulation (Ganachaud and Wunsch 2000; Lumpkin and Speer 2003), and the subtropical cell connecting the subduction regions of the subtropics with the equatorial upwelling (McCreary and Lu 1994; Schott et al. 2004).

The Atlantic EUC undergoes a strong seasonal cycle with vertical excursions mainly associated with the vertical movement of the thermocline as revealed by moored observations at the equator (Provost et al. 2004; Giarolla et al. 2005; Brandt et al. 2006). Earlier moored observations from February 1983 to October 1985, while showing a seasonally varying vertical migration of the EUC core, could not reveal a repeated seasonal cycle of the EUC transport due to pronounced interannual variability (Weisberg et al. 1987). Shipboard observations are still inconclusive concerning the seasonal cycle of the Atlantic EUC transport mainly due to the presence of large intraseasonal variability associated with tropical instability waves (TIWs) and wind-generated Kelvin waves (Bunge et al. 2007; Athie and Marin 2008; Han et al. 2008; Polo et al. 2008; Hormann and Brandt 2009).

In the Pacific Ocean, the strong interannual variations associated with El Niño/Southern Oscillation (ENSO) include strong EUC transport fluctuations with observed weakening or even disappearance of the EUC during El Niño phases (Firing et al. 1983; Johnson et al. 2002). The interannual variability of the Atlantic EUC was studied mainly by numerical models suggesting a similar weakening (strengthening) of the EUC during warm (cold) events (Goes and Wainer 2003; Hormann and Brandt 2007). As part of the Tropical Atlantic Climate Experiment (TACE), a program envisioned to enhance the observational network and to improve predictions of tropical Atlantic climate variability, subsurface moorings were installed at and near the equator at different longitudes. In the central Atlantic at 23°W, moored velocity observations started in December 2001 (Provost et al. 2004; Bunge et al. 2008). Almost continuous moored velocity observations (until today, but with a gap from December 2002 to February 2004) revealed the existence of equatorial deep jets (EDJs) at intermediate depths oscillating at a period of about 4.5 years (Johnson and Zhang 2003; Bunge et al. 2008; Brandt et al. 2011b). Because EDJs are characterized by downward phase and corresponding upward energy propagation, Brandt et al. (2011b) concluded that they are able to modulate subsurface and surface equatorial zonal velocity, thus contributing to SST and associated atmospheric interannual variability.

In the present study, we will use additional information from moorings deployed at 23°W off the equator at 0°45′S/N as well as from 20 ship cruises along the 23°W meridian. The objective of this study is to investigate the seasonal to interannual variability of the EUC. A particular focus is on key characteristics of the current such as volume transport, core velocity, core depth, and core latitude. Data and applied methods are presented in Sect. 2, EUC variability as well as EUC interannual variability and its relation to tropical Atlantic variability are presented in Sect. 3. Finally, the results are summarized and discussed in Sect. 4.

2 Data and methods

2.1 Shipboard data

In this study, we use direct shipboard velocity observations along meridional sections crossing the equator between 23°W and 28°W. In total 20 sections of zonal velocity taken during different research cruises from 1999 to 2011 were analyzed. From these sections we selected a subarea with a latitudinal range from 1°12′S to 1°12′N and a depth range from 30 to 300 m. The subarea covers almost the full extent of the EUC and includes the locations of the three moorings that will be discussed in the next section. The velocity sections, which are well distributed with regard to the seasonal cycle, are averaged to obtain an EUC mean zonal velocity (Fig. 1). Uncertainties in the determination of a mean EUC are dominated by ocean variability, whereas instrumental error sources are of minor importance. The standard error of the mean zonal velocity, which is defined as the standard deviation divided by the square root of the degrees of freedom (number of ship sections), is in general smaller than 4 cm/s except in the near-surface layer, where it reaches up to 8 cm/s. The mean EUC core at

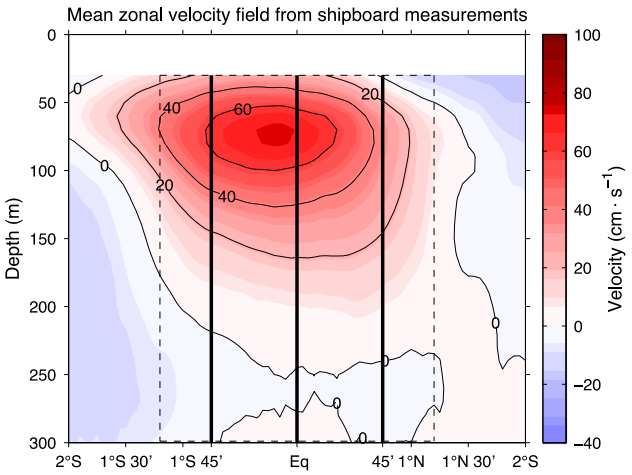

Fig. 1 Mean zonal velocity from 20 meridional ship sections taken from 1999 to 2011 between 23°W and 28°W. *Vertical black lines* mark the positions of moored observations, the *dashed box* marks the domain for which the velocity field will be reconstructed from moored observations

23°W is shifted slightly southward with respect to the equator to about 0°10′S and is located at a depth of about 87 m (Fig. 1). We assume that the shipboard zonal velocity sections, which do vary due to the presence of oceanic variability on intraseasonal to interannual time scales, contains the dominant EUC variability pattern. We will use in the following the dominant variability pattern of the zonal velocity from the shipboard velocity section to interpolate and extrapolate the moored observations.

2.2 Mooring data

The second dataset we use was obtained by an equatorial current meter mooring array along 23°W during the period May 2005 to June 2011. The mooring array consists of three moorings located at 0°45′S, equator, and 0°45′N, and was first deployed in June 2006, serviced in February 2008 and October 2009, and finally recovered in June 2011. To extend the available time series, we also use data from the equatorial current meter mooring deployed from May 2005 to June 2006. Data from the earliest mooring period from December 2001 to December 2002 was not used in the present study since the moored ADCP covered only the shallowest part of the EUC. During the later deployments, at the equatorial mooring two acoustic Doppler current profilers (ADCPs) were always installed: one 300 or 150 kHz upward looking instrument typically at a depth of about 150 m and another 75 kHz instrument either downward looking from just below the upper instrument or upward looking from larger depth. Data gaps between upward and downward looking instruments were interpolated. Unfortunately, the upper instrument failed during the mooring period June 2006 to February 2008 leading to a slightly reduced measurement range (Fig. 2). At the off-equatorial moorings, we used only upward looking instruments, either 150 kHz or 75 kHz leading to slightly varying depth ranges. All velocities were detided using a 40 h low-pass filter and subsampled to 12 h intervals. Velocity data from the equatorial mooring were previously used (1) to study the mean zonal flow, its seasonal cycle, as well as intraseasonal velocity fluctuations (Brandt et al. 2006), (2) to validate high-resolutions models used to analyze the generation of TIWs (von Schuckmann et al. 2008), and (3) to analyze the interannual variability of EDJs (Brandt et al. 2008, 2011b, 2012). Here, for the first time, we will use off-equatorial velocity time series to obtain an integral view on the seasonal to interannual variability of the EUC and its relation to tropical Atlantic variability.

2.3 Methods

2.3.1 Reconstruction of the velocity field using HEOFs

The goal here is to construct time series of two-dimensional (latitude–depth) velocity fields from moored zonal velocity data at three locations. The construction requires an interpolation between the moorings and an extrapolation toward the boundary of the domain. To avoid excessive

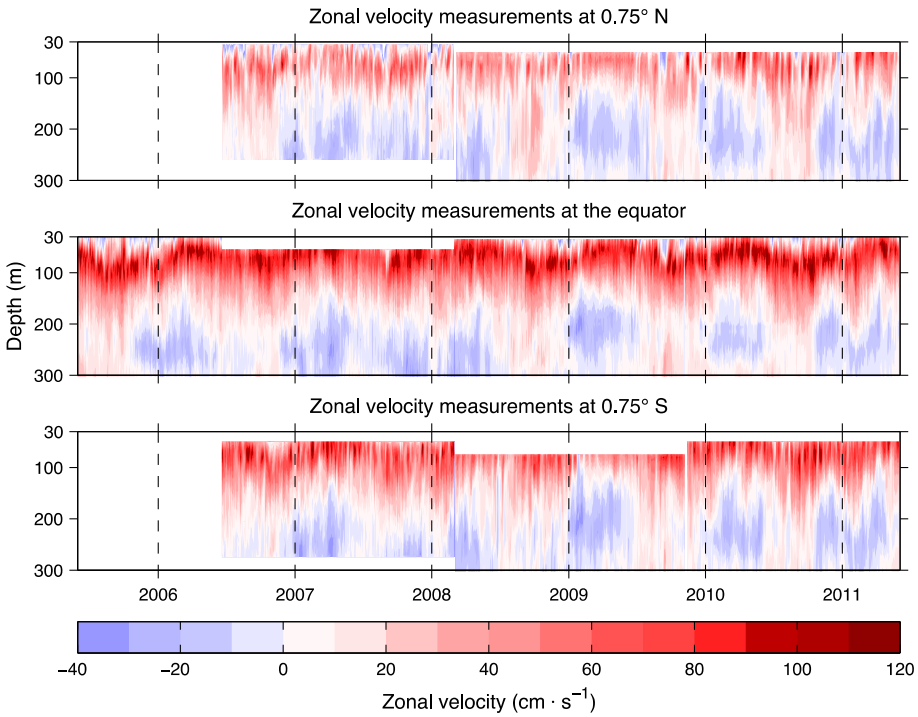

Fig. 2 Zonal velocity from moored observations at 0°45′N (*upper panel*), equator (*middle panel*) and 0°45′S (*lower panel*) acquired between May 2005 and June 2011

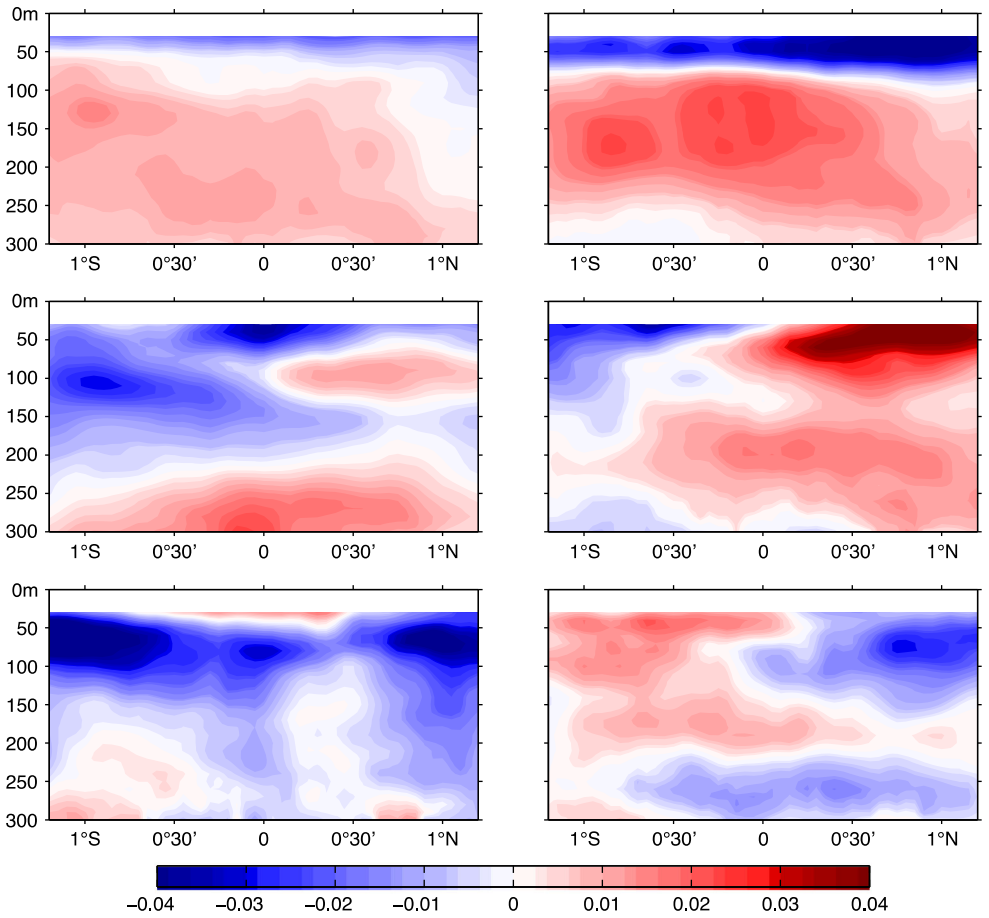

Fig. 3 First three HEOF patterns as calculated from 20 ship section. Row 1–3 corresponds to HEOF 1–3; *left/right column* corresponds to real/imaginary pattern. HEOF 1, 2, and 3 explains 55, 16, and 12 % of the variance contained in the shipboard velocity sections

poleward extrapolation of the velocity fields from the mooring positions located at 0°45′S/N, we restricted the latitudinal range of the domain to 1°12′S/N. The inter-/extrapolation scheme is based on the variability patterns obtained from the 20 available ship sections. Those ship sections are assumed to represent well the variability of the zonal velocity field of the EUC. Here, we apply the Hilbert transformation (Barnett 1983) to the zonal velocity fields of the ship sections

$$\mathbf{S20} = S20 + iH(S20) \quad (1)$$

where $S20$(y, z, t) is the three-dimensional velocity field with the spatial coordinates y and z being latitude and depth, and t referring to the time of the 20 ship sections, H is the Hilbert transform, and i the imaginary unit. By applying an empirical orthogonal function (EOF) analysis to **S20**, we obtained Hilbert EOFs (HEOFs) that are composed of real and imaginary pattern (Fig. 3). This technique is here more suitable than traditional EOF analysis because it is capable of detecting moving features in space, like e.g. north/south or up/down migration of the EUC core. The first three patterns explain 83 % of the variance contained in the ship sections. They are statistical patterns that nevertheless contain some features which correspond to EUC dynamics. For example, the first pattern that explains more than 50 % of the velocity variance describes a slightly tilted vertical motion of the velocity field; the second pattern describes a more latitudinal displacement of the EUC.

To reconstruct a vector field from the moored observations, a regression is done of the HEOF patterns onto the moored observations. To find the number of leading HEOFs to be used for the reconstruction, a good compromise has to be found between simplicity and explained variance. Here we will use the first three HEOFs composed of the six patterns shown in Fig. 3. A verification of this choice is presented in Sect. 2.3.3.

2.3.2 *Reconstruction of the EUC transport using the optimal width method*

When interested only in the EUC transport, here defined as the integral of u with $u > 0$ over latitude and depth within

the domain covering 30–300 m depth and 1°12′S–1°12′N, the optimal width (OW) method can be applied. This method is based on the calculation of the latitudinally integrated zonal velocity, $U(z, t)$, defined as the integral of u with $u > 0$ over a given latitude range. The principle of the method is to find optimal widths W_i such that:

$$U(z,t) = W_N u_N(z,t) + W_{eq} u_{eq}(z,t) + W_S u_S(z,t) \qquad (2)$$

where $u_i(z, t)$ are zonal velocities with the index N/S referring to the northern/southern mooring position at 0°45′N/S und the index eq to the equatorial mooring position. The constant widths W_i are calculated by regression of the latitudinally integrated zonal velocity from the ship sections onto the zonal velocities of the ship section at the three mooring positions. The obtained latitude ranges corresponding to W_N, W_{eq}, and W_S are 0.76, 0.74, and 0.79 degree latitude. In an equipartitioned domain each width would be 0.8 degree latitude. Consequently, the width of the equatorial mooring is underweighted and the sum of the three widths is less than the widths of the whole domain, which can be expected as the flow of the EUC becomes weaker toward the northern and southern boundary.

To reconstruct $U(z, t)$ from the mooring time series, zonal velocity measurements at each mooring position are required for the whole depth range (30–300 m). This is usually not the case (cf. Fig. 2). For instance, the depth range of the southern record covering the period June 2006 to February 2008 extends only from 50 to 275 m. Here we chose to fill such gaps that are also present during other mooring periods and at other locations with data obtained from the HEOF reconstruction. Integration of $U(z, t)$ over depth yields the EUC transport that can be compared with the reconstruction using the HEOF method.

2.3.3 Method validation

Here, we will use zonal velocity data from 20 meridional shipboard sections to validate the different methods applied to reconstruct full velocity sections (HEOF method) as well as EUC transport (HEOF and OW method) from moored observations. For this validation the zonal velocity data at the mooring positions are extracted from shipboard sections. The two methods are then applied to the extracted zonal velocity data and compared with results obtained from the full shipboard zonal velocity sections. We will only compare EUC transport values calculated from the ship sections with values from the reconstructions. The EUC transport used for the validation represents an integral value of the zonal velocity variability within the section and is less affected by oceanic variability on small spatial scales. Figure 4a shows the change in quality of the EUC transport calculation from the HEOF reconstruction when increasing the number of used HEOFs from one to three. The RMS difference between reconstructed and observed EUC transport reduces from 2.62 Sv when using only the first HEOF to 0.79 Sv when using the first three HEOFs, while the regression coefficient approaches 1 for larger numbers of used HEOFs. Using more than three HEOFs does not significantly improve the results. The RMS difference between reconstructed and observed zonal velocity when using the first three HEOFs is for most of the domain smaller than 5 cm/s with larger values (up to 15 cm/s) near

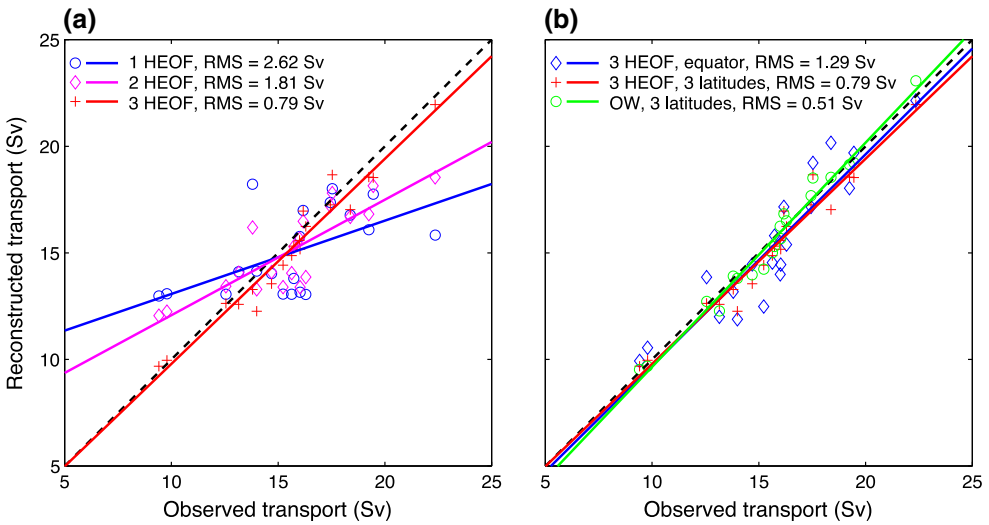

Fig. 4 Reconstructed versus observed EUC transport as calculated from shipboard zonal velocity data. **a** Reconstruction from zonal velocity data from the 3 mooring positions (0°45′N, eq., 0°45′S) using the first (*blue circles*), the first two (*purple diamonds*), and the first three (*red plus signs*) HEOFs. **b** Reconstruction from zonal velocity data from the equator only (*blue diamonds*) and from the 3 mooring positions (0°45′N, eq., 0°45′S) (*red plus signs*) using the HEOF method (first three HEOFs) and from the 3 mooring positions using the OW method (*green circles*). The *solid lines* in **a** and **b** are linear regressions with RMS values as given in the legend

the surface particularly near the northern and southern boundary of the domain.

For the mooring period May 2005–June 2006 only data from the equatorial mooring are available. We will use the HEOF method also in this case to reconstruct the full zonal velocity section. Figure 4b shows the quality of the HEOF reconstruction when using only data from the equator in comparison to the case when using data from 0°45′N, the equator, and 0°45′S. While the regression coefficient in both cases is similarly close to one, the RMS difference between reconstructed and observed EUC transport is clearly increased when using only equatorial data. Compared to the HEOF reconstruction the OW reconstruction results in a smaller RMS difference and in a regression coefficient even closer to one. In general, we can say that the OW method is more stable and slightly better reproduces EUC transport variability. However, the HEOF method additionally reconstructs the full zonal velocity field and thus allows studying further characteristics of the zonal velocity field within the whole domain such as maximum zonal velocity, latitude and depth of EUC.

Figure 5 shows time series of the EUC transport calculated using three different methods: (1) HEOF method with the first three HEOF applied to equatorial mooring data only, (2) HEOF method with the first three HEOF applied to data from all three moorings; and (3) OW method applied to data from all three moorings. As suggested by the method validation using shipboard velocity data, method 2 and 3 are very close; the RMS difference between both curves is RMS = 0.65 Sv, which can be understood as an uncertainty of the EUC transport calculation. Method 1 shows some systematic differences and increased RMS differences with respect to method 2 and 3: RMS = 1.07 Sv and RMS = 1.09 Sv, respectively. We particularly note an increase in the strength of intraseasonal fluctuations when using only equatorial mooring data for the reconstruction, the seasonal and interannual variability being less affected. Larger deviations between transport values from ship sections and reconstructions from moored observations (Fig. 5) are likely due to differences in methods used to derive these values: ship sections are snapshots that are completed during a day or two, while reconstructions are calculated from simultaneous and 40-h low-pass filtered moored velocity profiles. In the following we will use for the analysis of the seasonal cycle a 5 year-long time series (June 2006–June 2011) from both methods, method 2 and 3. For the analysis of interannual variability we will use a ∼6-year-long time series obtained from a combination of method 1 (May 2005–June 2006) and method 2 (June 2006–June 2011).

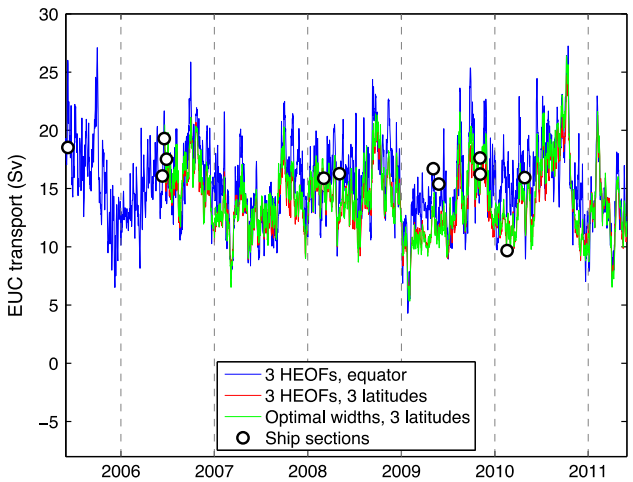

Fig. 5 EUC transport as calculated by applying the HEOF method with the first three HEOFs and using data from the equatorial mooring only (*blue line*) and from all three moorings (*red line*) and by applying the OW method and using data from all three moorings (*green line*). Also included are EUC transport values from meridional ship sections (*circles*)

3 Results

3.1 EUC variability at 23°W

Previous observational studies on the EUC variability in the Atlantic were based on single equatorial moorings (Provost et al. 2004; Giarolla et al. 2005; Brandt et al. 2006; Hormann and Brandt 2009). Here, we want to focus on seasonal to interannual variability of different EUC characteristics such as EUC transport (Fig. 6), EUC core depth (Fig. 7), EUC maximum core velocity (Fig. 8), and EUC core latitude (Fig. 9). The estimation of these characteristics requires additional information from off-equatorial moorings. The position of the core of the EUC is here defined as the mean velocity-weighted latitude and depth of all grid points with velocities larger than 20 cm/s. This definition is applied in order to produce more stable results for the core position than one would obtain by just picking the position of maximum velocity. A variation of the velocity threshold between 10 and 30 cm/s showed that the obtained results depend only weakly on the choice of this threshold: the mean EUC core moves slightly downward/upward and northward/southward for a smaller/larger threshold.

The EUC transport is dominated by a seasonal cycle ranging from about 18 Sv in boreal autumn (maximum in September) to about 12 Sv in late boreal winter (minimum in March). The absolute extremes of the EUC transport time series are in October 2010 with about 25 Sv and in February 2009 with about 5 Sv (Fig. 6a). The spectrum of the EUC transport time series (not shown) has enhanced energy in the 30–70 days period range. While at shorter

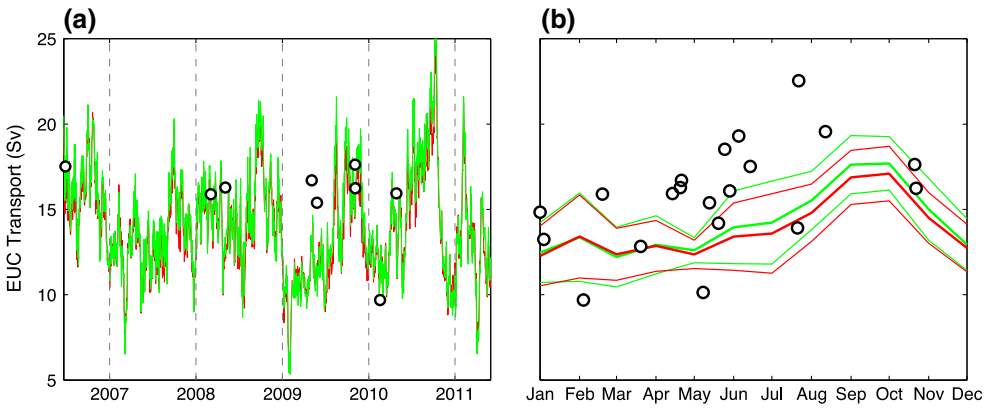

Fig. 6 **a** EUC transport and **b** its mean seasonal cycle with standard deviation of monthly means (*thin lines*) as obtained from the HEOF method (*red lines*) and the OW method (*green lines*). Shipboard measurements are marked by *circles*. The mean EUC transports from the HEOF and OW methods are 13.8 and 14.2 Sv, respectively

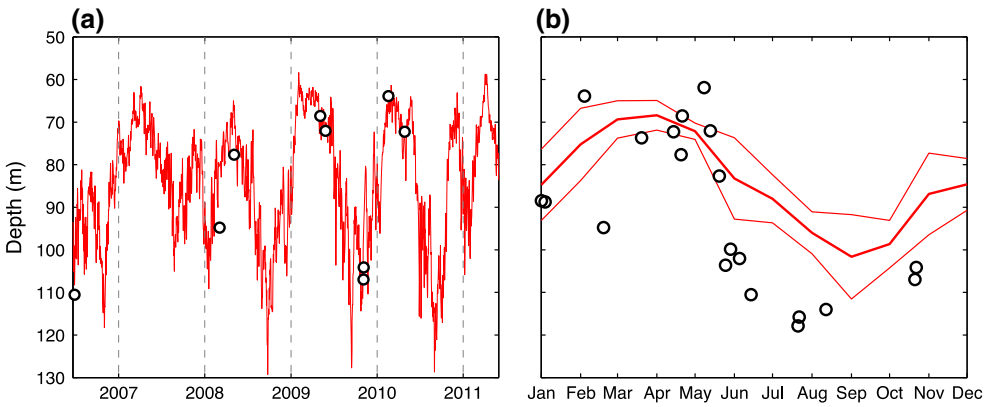

Fig. 7 **a** EUC core depth and **b** its mean seasonal cycle (*thick line*) with standard deviation of monthly means (*thin lines*) as obtained from the HEOF method. Shipboard measurements are marked by *circles*. The mean EUC core depth is 82 m

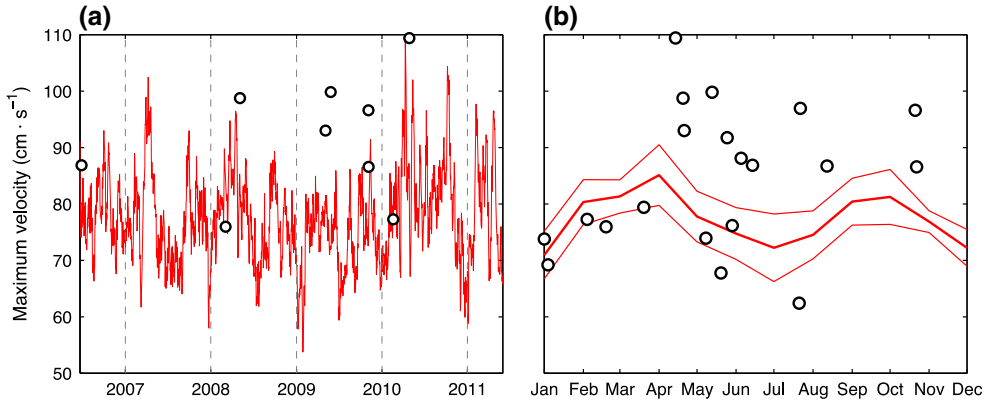

Fig. 8 **a** EUC maximum core velocity and **b** its mean seasonal cycle (*thick line*) with standard deviation of monthly means (*thin lines*) as obtained from the HEOF method. Shipboard measurements are marked by *circles*

periods (30–40 days) TIWs might play an important role (Brandt et al. 2006; Athie and Marin 2008), longer periods (50–70 days) were identified by Han et al. (2008) and Polo et al. (2008) to be associated with the presence of low baroclinic mode Kelvin waves. The strong intraseasonal fluctuations hamper the identification of the seasonal cycle of the EUC transport (and even more of its interannual variations) from shipboard observations (Fig. 6a). Shipboard observations show substantial variability during early boreal summer which is in general agreement with large standard deviation of monthly means from mooring data during the same season.

An even more pronounced seasonal cycle can be found for the EUC core depth (Fig. 7). As similarly found by analyzing only equatorial mooring data (Provost et al. 2004; Giarolla et al. 2005; Brandt et al. 2006), the EUC is shallowest during March/April and deepest during September. Deepest EUC in the shipboard dataset is found in

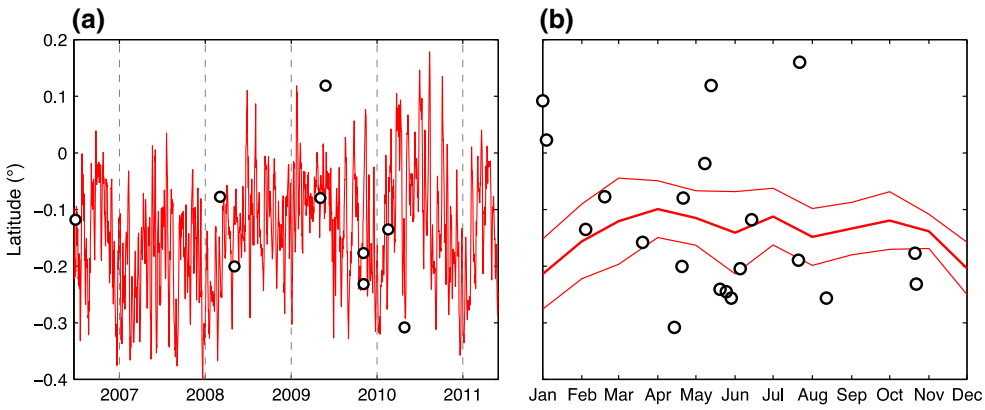

Fig. 9 **a** EUC core latitude and **b** its mean seasonal cycle (*thick line*) with standard deviation of monthly means (*thin lines*) as obtained from the HEOF method. Shipboard measurements are marked by *circles*

July/August with no measurements in September. Remarkable is the pronounced seasonal cycle of the EUC core depth in 2009 and 2010 and the weak seasonality in 2007. Years of strong (weak) seasonal cycle of EUC core depth do correspond to years with strong (weak) EUC transport seasonal cycle (cf. Figs. 6a, 7a). There seems to be a systematic difference between EUC core depth seasonal cycle from shipboard observations and moored observations during boreal summer and fall (Fig. 7b), but the few available shipboard sections do not unambiguously allow identifying the origin of this difference. In fact, boreal summer-fall is characterized by the largest standard deviation of monthly means, indicating strong year-to-year variations during that period. The July/August core depths from earlier ship sections, ranging between 110 and 120 m depth (Fig. 7b), are still in the range of values obtained from moored observations for July/August of the years 2008–2010 (Fig. 7a), indicating that the climatology derived from the shorter mooring period may not represent the true or 'typical' climatology of the core depth over a longer period of time. The quality of the reconstructed zonal velocity fields does not seem to be an issue since the comparison between shipboard and moored values for simultaneous measurements (Fig. 7a) shows generally good agreement between shipboard and moored EUC core depths.

The reconstruction of the zonal velocity field using the first three HEOFs inherently includes a smoothing of the velocity field. This becomes obvious when comparing observed and moored EUC maximum core velocities: values taken from reconstructed fields are in general biased low compared to values taken from shipboard sections. However, the time series of EUC maximum core velocity is dominated by intraseasonal fluctuations (Fig. 8a) with a weak semiannual cycle superimposed (Fig. 8b). Within the seasonal cycle maximum core velocities are found in April when the EUC core is shallowest and in September/October when the EUC core is deepest.

The mean EUC core is slightly shifted south with respect to the equator (Fig. 9): mean position is the same as obtained from the shipboard mean, i.e. 0°10′S. There is no clear seasonal cycle (EUC core is farthest south during December/January), but there is interannual variability in the latitudinal excursion of the EUC core with anomalous southward displacement during 2007 and anomalous northward displacement during 2009/2010 (Fig. 9).

3.2 Interannual variability and relation to tropical Atlantic variability (TAV)

To better understand the relation of the interannual EUC variability to TAV, we apply a regression analysis in which sea surface temperature (SST) and winds in the tropical Atlantic are regressed onto the EUC transport. Here we use monthly averages of NOAA–NCDC blended sea winds (http://www.ncdc.noaa.gov/oa/rsad/air-sea/seawinds.html) and TMI SST (http://www.ssmi.com/tmi/tmi_browse.html), both on a 0.25° resolution. As tropical Atlantic variability is strongly seasonally dependent (Sutton et al. 2000; Chang et al. 2006), we will perform regressions of monthly mean wind and SST of a specific month of the year onto monthly mean EUC transport for the same month (i.e. at zero lag) or for different months of the year corresponding to wind and SST leading the EUC. The EUC transport shows strongest variability during early boreal summer that corresponds to the onset of the equatorial Atlantic cold tongue (Caniaux et al. 2011).

From modeling studies (Goes and Wainer 2003; Hormann and Brandt 2007) and the analysis of few years of velocity data (Hormann and Brandt 2009) we expect that a strong (weak) EUC during boreal summer is associated with an anomalous cold (warm) equatorial Atlantic cold tongue. By using the 6 year-long moored time series, we will test this relation. We further want to test the importance of the preconditioning through zonal wind anomalies in the western equatorial Atlantic prior to the cold tongue

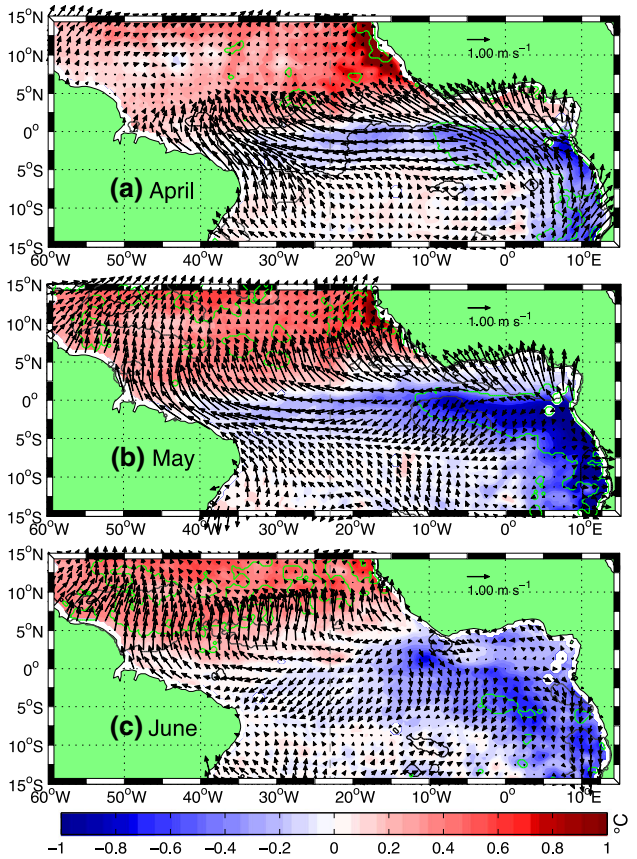

Fig. 10 Regression maps of SSTs (*color shading*) and winds (*arrows*) onto the June EUC transport normalized by its standard deviation. Regressions are calculated separately for wind and SST of the different months from April to June (**a**–**c**). Significant correlations (95 %) between June EUC transport and SSTs are marked by *green lines* and between June EUC transport and winds by *black lines*. There are 6 degrees of freedom corresponding to the number of available years of EUC transport data

season as suggested by Marin et al. (2009) and Hormann and Brandt (2009). Figure 10 shows the regression of wind and SST onto the June EUC transport. The regression maps show cold anomalies associated with a strong June EUC already during April (Fig. 10a), 2 months prior to the cold tongue season that begins in mid-June (Caniaux et al. 2011). During April the cold SST signal is more confined to the equator and the southeastern tropical Atlantic. With time progressing the cold anomaly intensifies in magnitude and extent. During May, maximum cold SST anomalies are found in the Atlantic cold tongue region (from about 10°W at the equator toward the African coast) and negative SST anomalies expand toward South America and the northern boundary of the Gulf of Guinea (Fig. 10b). Afterward cold anomalies further broaden southwestward, while maximum cold anomalies in the eastern equatorial Atlantic start to reduce (cf. Fig. 10b, c). The strongest wind anomalies associated with June EUC transport anomalies are found in April in the western equatorial Atlantic between 20°W and 40°W (Fig. 10a). Westward wind anomalies during April are associated with an anomalously strong EUC in June. In general, wind anomalies are found to be directed from regions of cold SST toward regions of warm SST (Fig. 10).

When regressing zonal velocities onto EUC transport at zero lag, it becomes evident that a strong EUC is in general associated with enhanced westward near-surface flow and enhanced eastward flow below the mean core of the EUC. These results confirm model results by Goes and Wainer (2003) suggesting greater (reduced) EUC transport associated with deeper (shallower) core depth. The mean shear between westward near-surface flow and eastward flow below is strongest during boreal summer (June) as indicated by the proximity of isolines of zonal velocity above the EUC core (Fig. 11). Besides stratification, the strength of vertical shear of the horizontal flow sets the strength of diapycnal mixing and downward heat flux (Hummels et al. 2013; Foltz et al. 2013; Jouanno et al. 2011a). Using the reconstructed zonal velocity fields along 23°W, we can show that the interannual variability in the strength of the shear is also strongest during boreal summer. Strong westward near-surface anomalies and strong eastward anomalies at the equator below the EUC core set the condition for enhanced diapycnal mixing during years of enhanced June EUC transport. During November, which corresponds to the period of secondary eastern equatorial Atlantic cooling in the seasonal cycle (Okumura and Xie 2006; Jouanno et al. 2011b), the shear enhancement is weaker than during June and its maximum is located farther south of the equator. It is mainly caused by a westward near-surface flow anomaly; the eastward flow anomaly below the EUC core is generally weaker. The seasonal cycle in the interannual shear variability suggests a stronger contribution of diapycnal mixing variability to interannual SST variability in the equatorial Atlantic during boreal summer compared to the rest of the year.

4 Summary and discussion

As part of the TACE program a current meter mooring array was installed in the equatorial Atlantic along 23°W for a 6-year period from 2005 to 2011. It was aimed to observe the seasonal to interannual variability of the EUC. Within the seasonal cycle the EUC transport is minimum in March and maximum in September. It shows a relatively slow increase from March to September and a more rapid decrease from October to December. The depth variations of the EUC core show a more harmonic cycle with shallowest EUC core in March and deepest EUC core in September. Seasonal variations of the maximum velocity of the EUC show instead a semiannual cycle with velocity

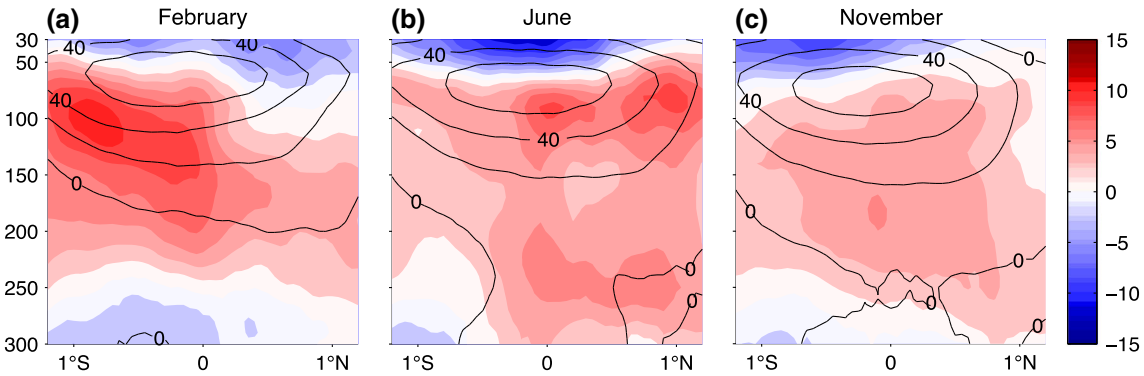

Fig. 11 Regression maps of zonal velocity (*color shading*, cm/s) onto EUC transport normalized by its standard deviation. Regressions are calculated at lag zero for **a** February, **b** June, and **c** November. Superimposed are the mean zonal velocities (cm/s) for the respective months in *black contours*

minima in January and July and velocity maxima in April and September. Due to strong decrease in the EUC cross-section, the EUC transport is smallest in spring during the phase of maximum core velocity.

The results regarding EUC core depth and maximum velocity are in general agreement with results obtained by analyzing a subset of the equatorial velocity time series (Provost et al. 2004; Brandt et al. 2006). Previous analyses of shipboard meridional velocity sections crossing the equator at different longitudes were not completely conclusive regarding the seasonal cycle of the EUC transport (Hormann and Brandt 2007; Kolodziejczyk et al. 2009). Shipboard measurements along 35°W showed maximum EUC transport values in September with an indication of a secondary maximum in April and large variability in early boreal summer (Hormann and Brandt 2007). The analysis of 18 shipboard sections at 10°W revealed a maximum EUC transport slightly earlier in the year during August and EUC transport minima during March and November, suggesting the presence of semiannual transport variations in addition to the dominant annual harmonic (Kolodziejczyk et al. 2009).

Arhan et al. (2006) analyzed the EUC seasonal variability in a general circulation model. They found an EUC transport maximum during boreal summer and autumn extending from the western boundary to about 5°W, which is in near-equilibrium with the strengthening of the equatorial Easterlies during the same season. The April maximum, which was in the simulations strongest west of 30°W and contrary to observations relatively stronger than the boreal summer/autumn maximum, was found to be the result of low-latitude wind curl forcing. At 23°W, the simulated seasonal variability that is characterized by a semiannual cycle with similar transport maxima in April and September/October (Arhan et al. 2006) overestimates the EUC transport during boreal spring with respect to observations (Fig. 6b). The simulations presented by Hormann and Brandt (2007) instead show a single transport maximum in September, which generally is in better agreement with the observations presented here. Note that the eastward transport calculations were performed in both cases (as well as in the observations) by excluding the upper 24–30 m of the water column with only weak changes identified when including the near-surface flow (Arhan et al. 2006).

During the TACE period from 2005 to 2011, we could observe substantial interannual variability (Fig. 12) with SST variations in the ATL3 box (20°W–0°, 3°S–3°N) of up to 2 °C particularly strong during early boreal summer (May–August). The western Atlantic (WATL) wind index (40°W–20°W, 3°S–3°N) showed maximum interannual variability during boreal spring (March to May) representing the period important for the preconditioning of the thermocline slope prior to the onset of the equatorial Atlantic cold tongue. Particularly extreme years were the year 2005 with coldest ATL3 SST anomalies on record from April to June and the year 2008 with warmest anomalies from June to August. The year 2005 had strongest boreal summer EUC transport consistent with strongest preconditioning by the WATL wind. During 2008 instead, weakest boreal spring WATL winds were present associated with relatively weak boreal summer EUC transport (Fig. 12). The role of the preconditioning for the cold event in 2005 was discussed by Hormann and Brandt (2009) and Marin et al. (2009), while Marin et al. (2009) highlighted additionally the role of intraseasonal wind fluctuations favoring the early cold tongue onset in 2005 likely due to enhanced wind induced diapycnal mixing. These 2 years can be understood as dominating the regression plots (Fig. 10) due to the shift of about 1 month in the onset of the Atlantic cold tongue, i.e. May 19th 2005 versus June 21st 2008 (onset dates derived by Caniaux et al. (2011)).

The year 2009 was an anomalous year, that according to the definition by Richter et al. (2013) can be understood as being close to a non-canonical cold event. Such an event is characterized by anomalous weak boreal spring WATL wind and accordingly weak preconditioning. The ATL3 SST was warmest during April/May 2009, but developed a record cooling from May to July 2009, and finally reached coldest ATL3 SST on record in August 2009 (Fig. 12b). Foltz and McPhaden (2010) suggested a wave response involving upwelling equatorial Rossby waves generated by wind curl anomalies associated with the interhemispheric meridional SST gradient. The reflection of the Rossby wave and eastward propagating Kelvin wave were hypothesized to be responsible for the anomalous cooling in the eastern equatorial Atlantic. To explain the non-canonical behavior, Richter et al. (2013) instead suggested an important role of meridional and zonal advection transporting temperature anomalies from the northern tropical Atlantic into the equatorial region. Our observations show that the strong cooling of the ATL3 SST from May to July 2009 was associated with the smallest EUC transport from January to July in the whole observational period (Fig. 12a). Such behavior is contrary to the usual behavior of the warm and cold event in 2005 and 2008, respectively, that are according to Richter et al. (2013) canonical warm and cold events. However, the anomalous weak EUC during the first half of 2009 might be traced back to the anomalous wind forcing associated with the strong meridional mode event (Foltz et al. 2012). The wind anomalies during January-to-April 2009 were characterized by an eastward equatorial wind anomaly in the center of the basin, northerly wind anomalies in the western part of the basin, and weaker wind curl pattern associated with a weaker meridional wind curl gradient across the equator compared to the mean January-to-April winds (Fig. 13).

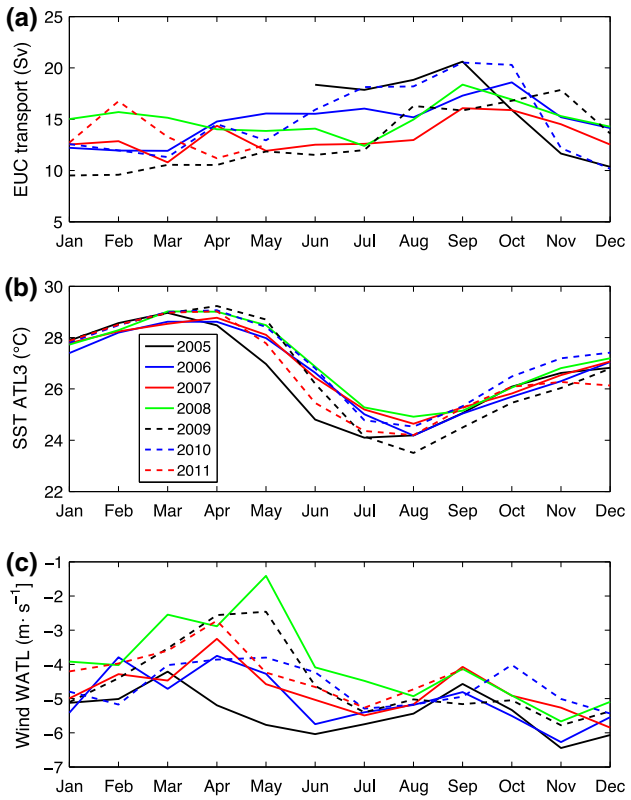

Fig. 12 Seasonal cycles of **a** EUC transport at 23°W, **b** ATL3 SST index (20°W–0°, 3°S–3°N), and **c** western Atlantic (WATL) wind index (40°W–20°W, 3°S–3°N) for the different years from 2005 to 2011. Different years are marked by *different line styles* as given in the legend in **b**

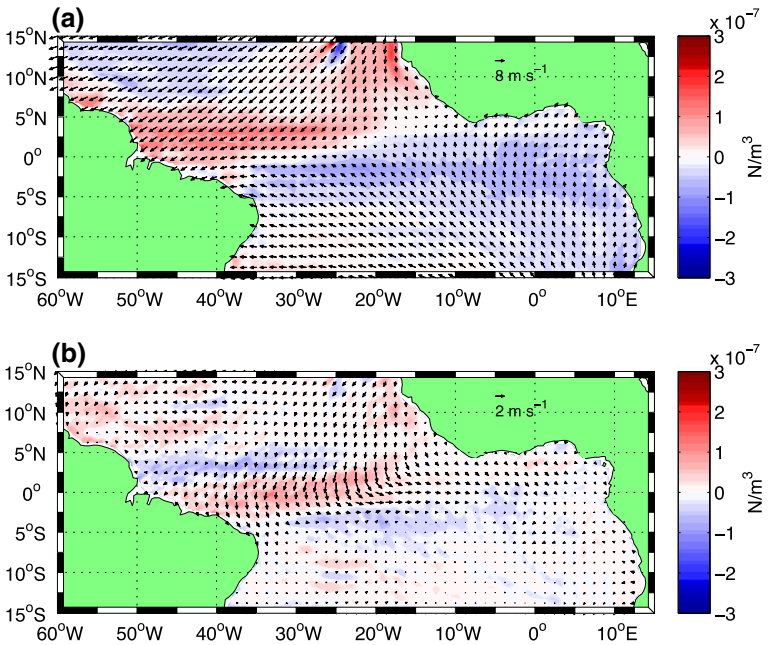

Fig. 13 **a** January-to-April mean wind (*arrows*) and wind stress curl (*color shading*) averaged for the period 2005–2011 and **b** corresponding 2009 anomalies

While eastward zonal wind anomalies are in general agreement with an anomalous weak EUC (Philander and Pacanowski 1980), northerly winds are found to be associated with an eastward surface and subsurface flow anomaly at the equator (Philander and Pacanowski 1981). The anomalous wind curl pattern is associated with a reduced eastward Sverdrup flow along the equator (Arhan et al. 2006; Kessler et al. 2003) and thus again in general agreement with an anomalous weak EUC during the same period. However, an attribution of the anomalously weak EUC during the first half of 2009 to different aspects of the wind forcing is beyond the scope of the present paper.

As a last point, we want to mention the meridional migration of the EUC core. This EUC characteristic shows only weak seasonality, but instead stronger interannual variations with an anomalous southward position of the EUC core during 2007 and an anomalous northward position during 2009/2010 (Fig. 9). The timescale of such variability would be in general agreement with the 4.5-year deep jet cycle (Brandt et al. 2011b) that was found to be consistent with equatorial basin mode oscillations (Greatbatch et al. 2012). However, to study low-frequency EUC variability that might result from the interaction of EDJs propagating their energy upward with the energetic near-surface flow, longer moored time series and/or improved numerical simulations are required.

Acknowledgments This study was funded by the Deutsche Bundesministerium für Bildung und Forschung (BMBF) as part of the projects NORDATLANTIK (03F0443B), RACE (03F0651B), MIKLIP (01LP1114A) and by the Deutsche Forschungsgemeinschaft through several research cruises with RV Meteor and RV Maria S. Merian and as part of the Sonderforschungsbereich 754 "Climate–Biogeochemistry Interactions in the Tropical Ocean". Moored velocity observations were acquired in cooperation with the PIRATA project. We would like to thank Verena Hormann and Ingo Richter for helpful discussion and two anonymous reviewers for their comments that lead to significant improvements in the manuscript.

References

Arhan M, Treguier AM, Bourles B, Michel S (2006) Diagnosing the annual cycle of the equatorial undercurrent in the Atlantic Ocean from a general circulation model. J Phys Oceanogr 36(8):1502–1522. doi:10.1175/Jpo2929.1

Athie G, Marin F (2008) Cross-equatorial structure and temporal modulation of intraseasonal variability at the surface of the Tropical Atlantic Ocean. J Geophys Res Oceans 113(C8). doi:10.1029/2007jc004332

Barnett TP (1983) Interaction of the monsoon and Pacific trade-wind system at interannual time scales. Part I: the equatorial zone. Mon Weather Rev 111(4):756–773. doi:10.1175/1520-0493(1983)111<0756:Iotmap>2.0.Co;2

Brandt P, Schott FA, Provost C, Kartavtseff A, Hormann V, Bourles B, Fischer J (2006) Circulation in the central equatorial Atlantic: mean and intraseasonal to seasonal variability. Geophys Res Lett 33(7). doi:10.1029/2005gl025498

Brandt P, Hormann V, Bourles B, Fischer J, Schott FA, Stramma L, Dengler M (2008) Oxygen tongues and zonal currents in the equatorial Atlantic. J Geophys Res Oceans 113(C4). doi:10.1029/2007jc004435

Brandt P, Caniaux G, Bourles B, Lazar A, Dengler M, Funk A, Hormann V, Giordani H, Marin F (2011a) Equatorial upper-ocean dynamics and their interaction with the West African monsoon. Atmos Sci Lett 12(1):24–30

Brandt P, Funk A, Hormann V, Dengler M, Greatbatch RJ, Toole JM (2011b) Interannual atmospheric variability forced by the deep equatorial Atlantic Ocean. Nature 473(7348):497–500. doi:10.1038/Nature10013

Brandt P, Greatbatch RJ, Claus M, Didwischus SH, Hormann V, Funk A, Hahn J, Krahmann G, Fischer J, Kortzinger A (2012) Ventilation of the equatorial Atlantic by the equatorial deep jets. J Geophys Res Oceans 117. doi:10.1029/2012jc008118

Bunge L, Provost C, Kartavtseff A (2007) Variability in horizontal current velocities in the central and eastern equatorial Atlantic in 2002. J Geophys Res Oceans 112(C2). doi:10.1029/2006jc003704

Bunge L, Provost C, Hua BL, Kartavtseff A (2008) Variability at intermediate depths at the equator in the Atlantic ocean in 2000–06: annual cycle, equatorial deep jets, and intraseasonal meridional velocity fluctuations. J Phys Oceanogr 38(8):1794–1806. doi:10.1175/2008jpo3781.1

Caniaux G, Giordani H, Redelsperger JL, Guichard F, Key E, Wade M (2011) Coupling between the Atlantic cold tongue and the West African monsoon in boreal spring and summer. J Geophys Res Oceans 116. doi:10.1029/2010jc006570

Chang P, Yamagata T, Schopf P, Behera SK, Carton J, Kessler WS, Meyers G, Qu T, Schott F, Shetye S, Xie SP (2006) Climate fluctuations of tropical coupled systems—the role of ocean dynamics. J Clim 19(20):5122–5174. doi:10.1175/Jcli3903.1

Cromwell T, Montgomery RB, Stroup ED (1954) Equatorial undercurrent in Pacific Ocean revealed by new methods. Science 119(3097):648–649. doi:10.1126/Science.119.3097.648

Firing E, Lukas R, Sadler J, Wyrtki K (1983) Equatorial Undercurrent disappears during 1982–1983 El-Nino. Science 222(4628):1121–1123. doi:10.1126/Science.222.4628.1121

Foltz GR, McPhaden MJ (2010) Abrupt equatorial wave-induced cooling of the Atlantic cold tongue in 2009. Geophys Res Lett 37. doi:10.1029/2010gl045522

Foltz GR, McPhaden MJ, Lumpkin R (2012) A strong Atlantic Meridional Mode event in 2009: the role of mixed layer dynamics. J Clim 25(1):363–380. doi:10.1175/Jcli-D-11-00150.1

Foltz GR, Schmid C, Lumpkin R (2013) Seasonal cycle of the mixed layer heat budget in the northeastern tropical Atlantic Ocean. J Clim 26(20):8169–8188. doi:10.1175/JCLI-D-13-00037.1

Ganachaud A, Wunsch C (2000) Improved estimates of global ocean circulation, heat transport and mixing from hydrographic data. Nature 408(6811):453–457. doi:10.1038/35044048

Giarolla E, Nobre P, Malagutti M, Pezzi LP (2005) The Atlantic equatorial undercurrent: PIRATA observations and simulations with GFDL Modular Ocean model at CPTEC. Geophys Res Lett 32(10). doi:10.1029/2004gl022206

Goes M, Wainer I (2003) Equatorial currents transport changes for extreme warm and cold events in the Atlantic Ocean. Geophys Res Lett 30(5). doi:10.1029/2002gl015707

Greatbatch RJ, Brandt P, Claus M, Didwischus SH, Fu Y (2012) On the width of the equatorial deep jets. J Phys Oceanogr 42(10):1729–1740. doi:10.1175/Jpo-D-11-0238.1

Han WQ, Webster PJ, Lin JL, Liu WT, Fu R, Yuan DL, Hu AX (2008) Dynamics of intraseasonal sea level and thermocline variability in the equatorial Atlantic during 2002–03. J Phys Oceanogr 38(5):945–967. doi:10.1175/2008jpo3854.1

Hormann V, Brandt P (2007) Atlantic Equatorial Undercurrent and associated cold tongue variability. J Geophys Res Oceans 112(C6). doi:10.1029/2006jc003931

Hormann V, Brandt P (2009) Upper equatorial Atlantic variability during 2002 and 2005 associated with equatorial Kelvin waves. J Geophys Res Oceans 114. doi:10.1029/2008jc005101

Hummels R, Dengler M, Bourlès B (2013) Seasonal and regional variability of upper ocean diapycnal heat flux in the Atlantic cold tongue. Prog Oceanogr 111:52–74. doi:10.1016/j.pocean.2012.11.001

Johnson GC, Zhang DX (2003) Structure of the Atlantic Ocean equatorial deep jets. J Phys Oceanogr 33(3):600–609. doi:10.1175/1520-0485(2003)033<0600:Sotaoe>2.0.Co;2

Johnson GC, Sloyan BM, Kessler WS, McTaggart KE (2002) Direct measurements of upper ocean currents and water properties across the tropical Pacific during the 1990s. Prog Oceanogr 52(1):31–61. doi:10.1016/S0079-6611(02)00021-6

Jouanno J, Marin F, du Penhoat Y, Molines JM, Sheinbaum J (2011a) Seasonal modes of surface cooling in the Gulf of Guinea. J Phys Oceanogr 41(7):1408–1416. doi:10.1175/Jpo-D-11-031.1

Jouanno J, Marin F, du Penhoat Y, Sheinbaum J, Molines JM (2011b) Seasonal heat balance in the upper 100 m of the equatorial Atlantic Ocean. J Geophys Res Oceans 116. doi:10.1029/2010jc006912

Kessler WS, Johnson GC, Moore DW (2003) Sverdrup and nonlinear dynamics of the Pacific equatorial currents. J Phys Oceanogr 33(5):994–1008. doi:10.1175/1520-0485(2003)033<0994:Sandot>2.0.Co;2

Kolodziejczyk N, Bourles B, Marin F, Grelet J, Chuchla R (2009) Seasonal variability of the equatorial undercurrent at 10 degrees W as inferred from recent in situ observations. J Geophys Res Oceans 114. doi:10.1029/2008JC004976

Lumpkin R, Speer K (2003) Large-scale vertical and horizontal circulation in the North Atlantic Ocean. J Phys Oceanogr 33(9):1902–1920

Marin F, Caniaux G, Bourles B, Giordani H, Gouriou Y, Key E (2009) Why were sea surface temperatures so different in the eastern equatorial Atlantic in June 2005 and 2006? J Phys Oceanogr 39(6):1416–1431. doi:10.1175/2008jpo4030.1

McCreary JP, Lu P (1994) Interaction between the subtropical and equatorial ocean circulations—the subtropical cell. J Phys Oceanogr 24(2):466–497

Metcalf WG, Voorhis AD, Stalcup MC (1962) The Atlantic equatorial undercurrent. J Geophys Res 67(6):2156–2202. doi:10.1029/JZ067i006p02499

Okumura Y, Xie SP (2006) Some overlooked features of tropical Atlantic climate leading to a new Nino-like phenomenon. J Clim 19(22):5859–5874. doi:10.1175/Jcli3928.1

Philander SGH, Pacanowski RC (1980) The generation of equatorial currents. J Geophys Res Oceans 85(Nc2):1123–1136. doi:10.1029/Jc085ic02p01123

Philander SGH, Pacanowski RC (1981) The oceanic response to cross-equatorial winds (with application to coastal upwelling in low latitudes). Tellus 33(2):201–210

Polo I, Lazar A, Rodriguez-Fonseca B, Arnault S (2008) Oceanic Kelvin waves and tropical Atlantic intraseasonal variability: 1. Kelvin wave characterization. J Geophys Res Oceans 113(C7). doi:10.1029/2007jc004495

Provost C, Arnault S, Chouaib N, Kartavtseff A, Bunge L, Sultan E (2004) TOPEX/Poseidon and Jason equatorial sea surface slope anomaly in the Atlantic in 2002: comparison with wind and current measurements at 23 W. Mar Geod 27(1–2):31–45. doi:10.1080/01490410490465274

Qiao L, Weisberg RH (1997) The zonal momentum balance of the equatorial undercurrent in the central Pacific. J Phys Oceanogr 27(6):1094–1119

Richter I, Behera SK, Masumoto Y, Taguchi B, Sasaki H, Yamagata T (2013) Multiple causes of interannual sea surface temperature variability in the equatorial Atlantic Ocean. Nat Geosci 6(1):43–47. doi:10.1038/Ngeo1660

Schott FA, Fischer J, Stramma L (1998) Transports and pathways of the upper-layer circulation in the western tropical Atlantic. J Phys Oceanogr 28(10):1904–1928

Schott FA, Mccreary JP, Johnson GC (2004) Shallow overturning circulations of the tropical–subtropical oceans. In: Wang C, Xie S-P, Carton JA (eds) Earth climate: The ocean–atmosphere interaction. Geophys Monogr 147. American Geophysical Union, Washington, DC, pp 261–304

Sutton RT, Jewson SP, Rowell DP (2000) The elements of climate variability in the tropical Atlantic region. J Clim 13(18):3261–3284. doi:10.1175/1520-0442(2000)013<3261:Teocvi>2.0.Co;2

von Schuckmann K, Brandt P, Eden C (2008) Generation of tropical instability waves in the Atlantic Ocean. J Geophys Res Oceans 113(C8). doi:10.1029/2007jc004712

Weisberg RH, Hickman JH, Tang TY, Weingartner TJ (1987) Velocity and temperature observations during the seasonal response of the Equatorial Atlantic Experiment at 0°, 28°W. J Geophys Res Oceans 92(C5):5061–5075. doi:10.1029/Jc092ic05p05061